A 3-Axis Surface Micromachined ΣΔ Accelerometer

Regular Paper - Session 12.4

Mark A. Lemkin
U.C. Berkeley, Doctoral Candidate,
497 Cory Hall, University of California, Berkeley CA, 94720
Phone (510) 642-8713, Fax: (510) 643-6637
email: lemkin@kowloon.eecs.berkeley.edu

Monico A. Ortiz,
U.C. Berkeley, Graduate Student

Naiyavudhi Wongkomet,
U.C. Berkeley, Doctoral Candidate

Bernhard E. Boser
U.C. Berkeley, Assistant Professor

James H. Smith
Sandia National Laboratories, Senior Member Technical Staff

This paper describes a monolithic 3-axis surface micromachined accelerometer with capacitive sense and feedback circuitry. The 3-axis sensor uses three separate proof masses to measure acceleration. Each proof mass has its own set of interface circuitry, all of which are coordinated by an on-chip master clock. By including x-, y-, and z-axis sensors on one chip, this accelerometer provides a single-chip solution for measuring three of the six degrees of freedom needed in an inertial measurement unit.

Accelerations applied to the die cause displacement of the proof mass relative to the substrate. Air gap capacitors formed between the proof mass and stationary terminals are used both for position sensing and force feedback. Since the position sense circuitry must be able to detect fractions of an attoFarad change in capacitance, a sense element with differential output enabling the use of fully differential circuitry is desired. Figure 1 shows a photograph of the 3 sense elements used to measure acceleration in the x-, y-, and z-axes. The x- and y-sense elements are realized with a differential comb finger array [1], while the z-axis sense element consists of a parallel plate capacitor formed between the proof mass and a layer of ground plane polysilicon [2]. Because this device has only one structural poly layer, a single z-axis sense element is unable to provide differential output. Fully differential z-axis output is achieved with a stiffly anchored reference capacitor, C_{zref}, in conjunction with the z-axis sense element. In order to fit all three devices in the allotted space, the y-axis proof mass is about half as large as the x-axis proof mass.

The proof mass is enclosed in an electromechanical $\Sigma\Delta$ feedback loop, providing force balancing in addition to A/D conversion of the input acceleration. This second order system is unstable without compensation. Reference [3] achieves stability by overdamping a bulk-micromachined

proof mass, moving one pole above the feedback loop bandwidth. This method is not desirable in surface micromachined sensors due to the associated increase in Brownian noise. References [1, 2] stabilize the system through a FIR lead filter in the feedback path. Due to the need for a multi-bit DAC in the feedback path, this method suffers from reduced linearity and dynamic range. By locating the compensator in the forward path, shown in Figure 2, these drawbacks are avoided.

Operation of the $\Sigma\Delta$ loop occurs in five phases: *feedback*, *zero*, *sense a*, *sense b*, and *compare*. Figure 3 shows a schematic diagram of the sense element and position sense interface. Figure 4 shows a system timing diagram. During the *feedback* phase the opamp input is disconnected from the sense element, and the input and output terminals of the opamp are zeroed. One-bit electrostatic force feedback is applied by grounding the proof mass and applying a reference voltage to the stationary terminal of either C_{s+} or C_{s-}, while holding the other capacitor at ground. During the *zero* phase, charge on the sense capacitors is removed before being connected to the charge integrator. In the first sense phase, *sense a*, a positive voltage pulse of magnitude V_{s+} is applied to the proof mass. The integrator output includes the position signal due to differences in C_s as well as errors from opamp offset, 1/f noise, charge injection mismatch, and kT/C noise from switches S_1 and S_2. This output is amplified by the preamp and sampled on capacitors C_h. During the second sense phase, *sense b*, the capacitors C_h are disconnected from ground and a negative voltage of magnitude V_{s-} is applied to the proof mass. The output is taken as the top plate voltage of C_h, performing a differencing operation on the preamp output during Φ_{sa} and Φ_{sb}. Since errors remain constant over Φ_{sa} and Φ_{sb}, they are canceled while the position signal is doubled. Because the integrator has a gain of only 7 μV/mg, several stages of preamps are used to boost the signal before the compensator.

Since both C_{s+} and C_{s-} are driven with the same voltage, input common-mode feedback (ICMFB) is needed to keep common-mode voltage at the opamp input constant. ICMFB relaxes requirements on opamp input common-mode range, enabling use of large sense voltages which lower input referred noise. In addition, ICMFB reduces offset due to mismatches in parasitic capacitances C_p. Experimental results show an uncalibrated output offset due to mismatch in the sensor and electronics of 5% and 8% of full scale for the x- and y-axes respectively.

Figure 5 shows a schematic of the forward path compensator $H_c(z)$. This compensator realizes the discrete time FIR lead filter $2-z^{-1}$. After settling has occurred in phase *sense b*, the output from the preamp is sampled onto capacitors C_1 and capacitors C_2. During the *compare* phase C_1 is disconnected from the position sense output and connected to C_3 which stores position from the previous period, implementing the delay z^{-1}. C_1 is twice as large as C_2 and C_3 to realize the proper FIR filter coefficients. The minus sign is implemented by flipping the polarity of capacitors C_2 and C_3 in the *compare* phase. Quantization of the compensator output is accomplished with a regenerative latch. By enabling the latch half way through the compare phase, sufficient time is allotted for charge redistribution between sampling capacitors.

Figure 6 shows a die photograph of the complete 4mm x 4mm sensor. The mechanical structures are fabricated in a trench before the 2μm CMOS circuitry is defined [4]. The device operates from a 5V supply and uses a single phase clock input to generate all necessary clock phases on chip. For evaluation, the sensor is mounted on a shaker table and excited with sinusoidal accelerations. A reference accelerometer mounted on the test board is used for calibration. Table 1 summarizes

results of experimental measurements and system parameters. Differences in noise floor and dynamic range are due to different mechanical structures used in the x-, y- and z-axes. Compared to the lateral surface micromachined accelerometers reported in [1] and [5], the x-axis device provides an increase in dynamic range of 27 dB and 24 dB respectively.

Acknowledgments:

References:

[1] Lemkin, M., Boser B.E., "A micromachined fully differential lateral accelerometer," CICC Dig. Tech. Papers, May 1996, pp. 315-318.

[2] Lu, C., Lemkin, M., Boser, B.E., "A monolithic surface micromachined accelerometer with digital output," IEEE Journal of Solid State Circuits, pp. 1367-1373, Dec. 1995.

[3] Smith, T. et. al., "A 15b Electromechanical Sigma-Delta Converter for Acceleration Measurements," ISSCC Dig. Tech. Papers, pp. 160-161, 1994.

[4] Smith, J. H., et. al., "Embedded Micromechanical Devices for the Monolithic Integration of MEMS with CMOS," Proc. 1995 IEDM, pp. 609-612.

[5] Analog Devices, "ADXL05 - 1g to 5g Single Chip Accelerometer with Signal Conditioning,"

Datasheet, 1995, One Technology Way, Norwood, MA 02062.

Table 1: Measurement results and system parameters

Parameter	Value
Noise Floor	
X-Axis	110 μg / √Hz
Y-Axis	160 μg / √Hz
Z-Axis	990 μg / √Hz
Dynamic Range (100 Hz Bandwidth)	
X-Axis	84 dB
Y-Axis	81 dB
Z-Axis	70 dB
Proof Mass, Resonant Frequency	
X-Axis	0.375 μ-gram, 3.2 kHz
Y-Axis	0.259 μ-gram, 4.2 kHz
Z-Axis	0.389 μ-gram, 8.3 kHz
Die Size	4mm x 4mm
Technology	2 μm CMOS, Single 2 μm thick structural poly
Power Dissipation	9mA @ 5V per Axis
Sampling Rate	500 kHz

2mm

X-Axis Sense Element

Y-Axis Sense Element

Z-Axis Reference (C$_{Zref}$)
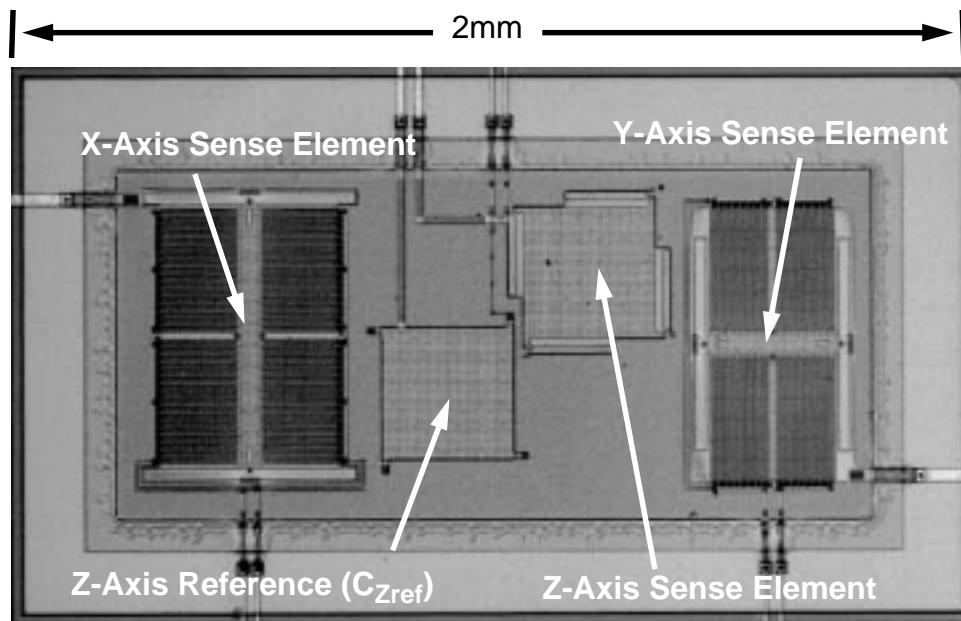
Z-Axis Sense Element

Figure 1: Photograph of sense elements
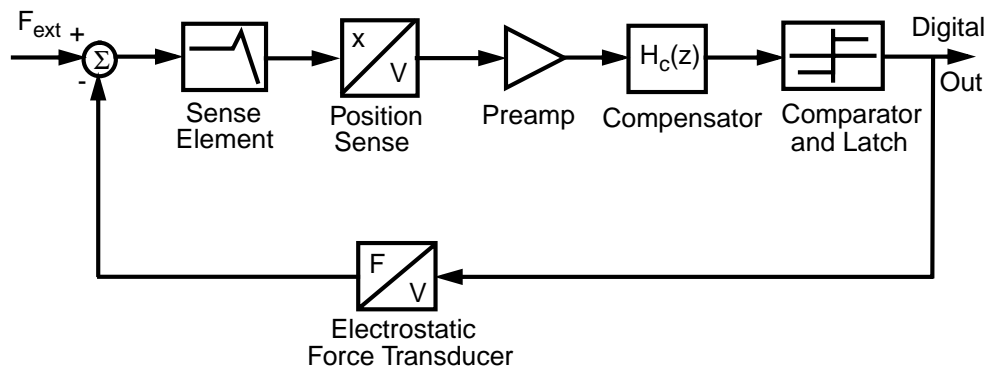
Figure 2: System diagram with forward path lead compensator

Figure 4: System timing diagram

OUT+

IN+

IN-

OUT-

$\Phi_{samp}*\Phi_{chop}$ $\Phi_{eval}*\overline{\Phi}_{chop}$ $\Phi_{samp}*\Phi_{chop}$ $\Phi_{eval}*\overline{\Phi}_{chop}$

$\Phi_{samp}*\overline{\Phi}_{chop}$ $\Phi_{eval}*\Phi_{chop}$ $\Phi_{samp}*\overline{\Phi}_{chop}$ $\Phi_{eval}*\Phi_{chop}$

Φ_{samp} Φ_{eval} Φ_{samp} Φ_{eval}

$C_1{}^+$ $C_2{}^+$ $C_3{}^+$ $C_1{}^-$ $C_2{}^-$ $C_3{}^-$
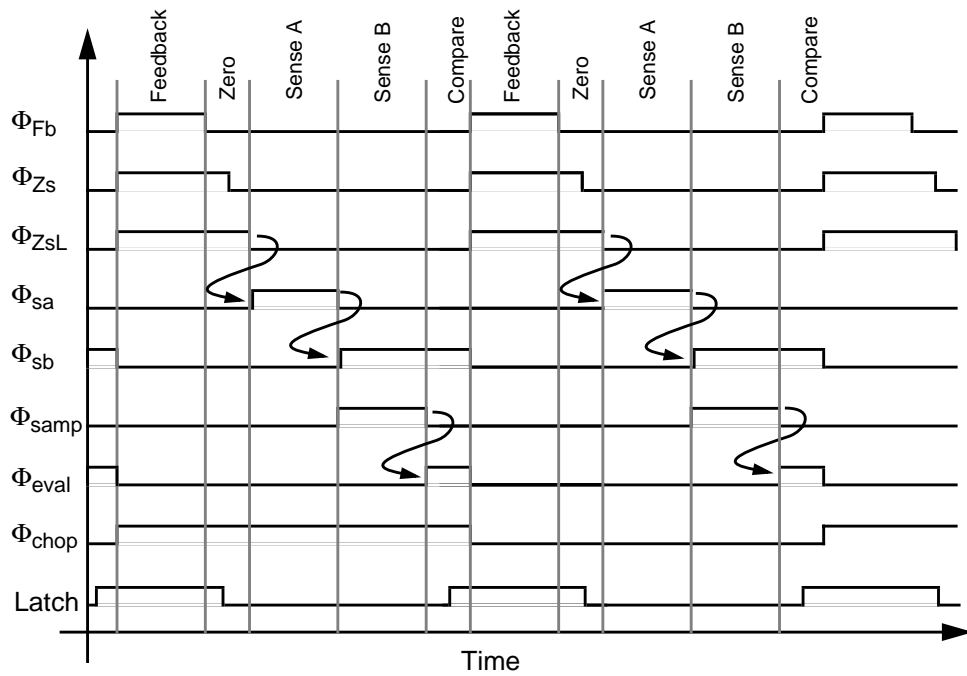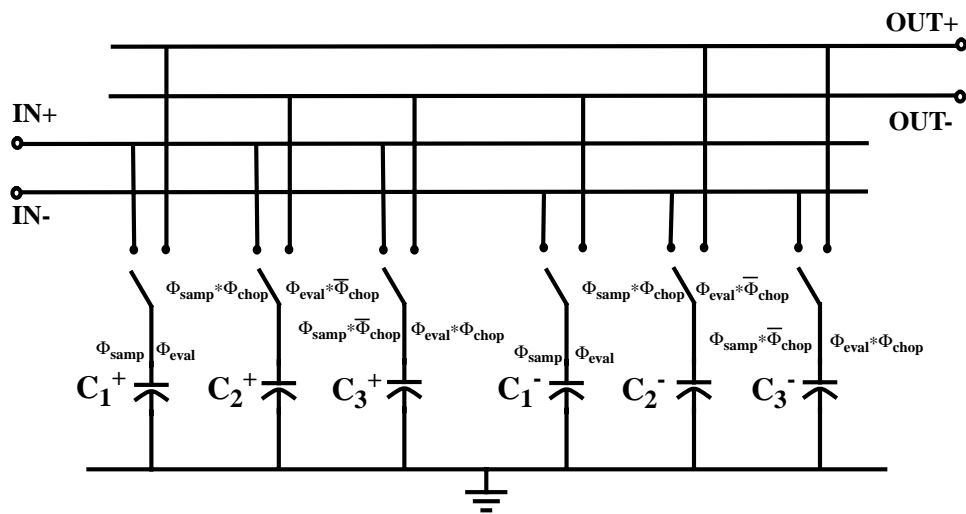
Figure 5:Schematic diagram of compensator

Figure Captions:

Figure 1: Photograph of sense elements

Figure 2: System diagram with forward path lead compensator

Figure 3: Schematic diagram of sense element and position sense interface

Figure 4: System timing diagram

Figure 5: Schematic diagram of compensator

Figure 6: Die photograph of 3-axis accelerometer